Two Dimensions Residual Stresses Analysis Through Incremental Groove Machining Combined with Electronic Speckle Pattern Interferometry

Guillaume Montay, Olivier Sicot, Afaf Maras, Emmanuelle Rouhaud, Manuel François

Two Dimensions Residual Stresses Analysis Through Incremental Groove Machining Combined with Electronic Speckle Pattern Interferometry

G. Montay, O. Sicot, A. Maras,
E. Rouhaud, M. François

Abstract In this study a new residual stress determination method in two directions simultaneously is presented. This method is based on stresses relaxation in a groove that is machined incrementally. The residual stresses relaxation occurs simultaneously from both the depth and the length of the groove. Thus, measuring the surface strain field generated by the relaxation enables to determine the stress gradient both along the depth and the length of the groove. To measure the surface strain in a direction perpendicular to the groove, a digital speckle pattern interferometer is used. This method is suitable when the residual stress field in the structure varies in the depth as well as along the surface of the part, like for example in a welded structure. The method is tested here on an aluminium plate in which a central band has been shot peened.

Keywords Residual stresses · Incremental groove machining method · Electronic Speckle Pattern Interferometry (ESPI) · Ultra-sonic shot peening · Aluminium

Introduction

Residual stresses are stresses that exist in a material without the action of external load (mechanical or thermal) [1]. Theses stresses are in self equilibrium and usually give no external manifestation. They are a result of the history of the part, generated by past heterogeneous plastic deformation, thermal contraction/expansion and phase transformation induced by manufacturing processes [2]. They combine to the service stresses and they can affect dramatically the performance of the materials such as fracture resistance, fatigue life, dimensional stability, quality of coatings, etc... Residual stresses can have detrimental or beneficial effects on the material behaviour according to their sign and amplitude. Generally, tensile stresses are detrimental and compressive stresses are beneficial. The design of new residual stress analysis methods is a challenge to progress in material science and technology. Knowing the magnitude and distribution of residual stresses is important to assess their effect on structural behaviour.

The majority of measurement methods (destructive or not) determine residual stress evolution in one direction (generally in depth or on the surface) [1, 3]. In many cases, knowing the residual stress evolution in only one direction is not sufficient. In the case of welded joints, the residual stress field is neither homogenous in depth nor along the transverse direction of the joint. Further, some structures are prestressed only on part of their surface, e.g. some turbine or fan blades can be LASER shock-peened on a fine band and the remaining of the structure is not affected directly by the process. More and more engineers tend to introduce residual stress very locally. Thus, the knowledge of the two dimensional distribution of residual stresses in the component is usually required.

In the present study, a new residual stress determination method in two simultaneous directions is presented. This method is based on the evaluation of the stress relaxation during the incremental machining of a groove. The residual stress relaxation occurs simultaneously from both the depth

G. Montay (✉) · O. Sicot · A. Maras · E. Rouhaud · M. François
Université de Technologie de Troyes (UTT),
Institut Charles Delaunay, LASMIS, FRE CNRS 2848,
12, rue Marie Curie, BP 2060,
10010 Troyes, France
e-mail: montay@utt.fr

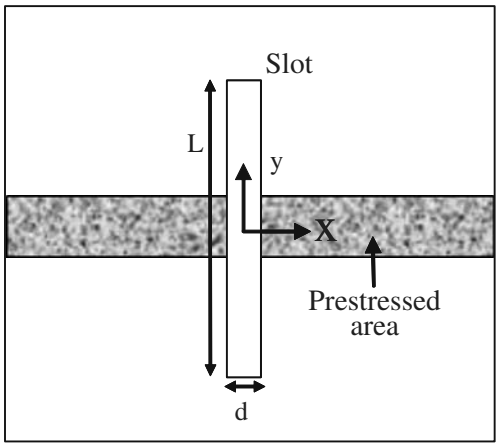

Fig. 1 Scheme of the groove, along axis *y*, machined in a localized prestressed area

and the length of the grove. Thus, by measuring surface displacement or strain fields generated by the relaxation, the stress gradient along both the depth and the length of the groove can be determined. To measure the surface displacements or the strains an optical interferometer is used because it gives full field information with a good resolution. Optical methods based on light interference have been developed for more than twenty years to measure mechanical fields (displacement, strain). Various techniques can be found, shearography or grating shearography to measure strains [4, 5] and ESPI or moiré interferometry to measure displacements [6–8]. In the present study, Electronic Speckle Pattern Interferometry (ESPI) with a phase shifting technique was chosen to measure surface displacements. This technique does not require surface preparation, provides a high resolution and a high sensitivity (about 100 nm in displacement) and is relatively simple to use.

Residual Stress Determination: Background

Several methods exist in the literature to determine residual stresses. All these techniques are complementary and can be classified as non destructive, semi-destructive and destructive.

Diffraction methods play an important part in residual stress measurements. They are based on the determination of elastic lattice strain [3]. X-ray diffraction is limited for in the depth investigation (several micrometers), when neutron or synchrotron techniques that allow in-depth evaluation are the most accurate methods but required costly heavy installations. Ultrasonic methods need an experimental calibration of the tested material which is not always easy to do [9, 10]. The incremental hole drilling method is well adapted for a large range of problems but it evaluates the residual stress profile only along the depth (one dimension) of the sample [11, 12]. The contour method is very well adapted for two dimensions analysis but this method is not easy to apply on large components and relies heavily on the geometrical quality of the cutting surface [13–16].

The method proposed in the present paper can be classified as semi-destructive, and gives the residual stress profile along two directions (along the depth and along another axis on the free surface). The method proposed in this paper is an evolution of the incremental hole drilling method and of the incremental slitting method [11, 17].

Principles of the Incremental Groove Machining Method

The semi-destructive incremental groove machining method (IGMM) is based on the stress relaxation principle. When a groove is machined in a prestressed component (Fig. 1), the residual stresses that were applied on the surface created by the groove relax and this generates surface displacements. The groove is drilled perpendicularly to the prestressed area. The measured displacement $U_x(x,y)$ is generated by the relaxation of the stress field that was in the removed part of the groove as described in Fig. 2.

The displacement $U_x(x,y)$ is not constant along direction y because the residual stresses are not homogeneous along the groove. It is important to note that each measured displacement $U_x(x,y)$ is due to the relaxation of the stress field in the groove as a whole, inducing a contribution of the stress along y and in the depth.

Other consequences of the stress field relaxation must be considered: the surface displacement, for a given depth increment, depends not only on the stress relaxation due to this increment but also on the stress in the previously removed layer. The new stress distribution between two

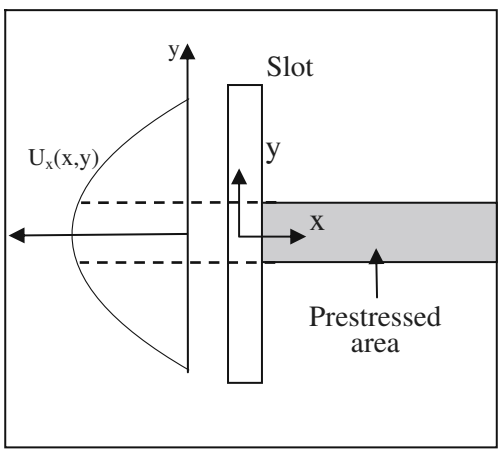

Fig. 2 Scheme of the displacement U_x distribution along the groove drilled for a given abscissa *x*

successive machining operations must be considered to determine the stress in the machined layer.

With this approach, the displacement field in the direction x is determined experimentally for a given abscissa x, along direction y for each depth increment. With the help of a finite element analysis, the residual stress field in directions y and z will be determined.

To measure the displacement perpendicularly to the groove, speckle interferometry combined with a phase shifting technique was used. This method gives the whole field of surface displacement in the direction of the sensitivity vector (along x in the present study).

Phase Shifting ESPI Applied to the Incremental Groove Drilling Method: Theory

Electronic Speckle Pattern Interferometry (ESPI) is a technique that is widely used to measure full-field deformation on surfaces of many kinds of objects [18–20]. ESPI is a non contacting surface displacement measurement method. This method is suitable for in plane displacements measurement and for rough surfaces. The speckle interferometer used in this study is a classical two beams interferometer [18, 19] depicted on Fig. 3.

In this study, a temporal phase shifting method is used [21]. The phase of one beam of the interferometer is shifted with a mirror mounted on a piezo-translator. A set of interference patterns corresponding to the given phase shifts is recorded. In the present study, five phase steps are recorded. For each phase step, the intensity $I^i(x, y)$ of a speckle pattern i is recorded:

$$I^i(x,y) = I_0(x,y)\left[1 + \gamma(x,y).\cos\left(\phi(x,y) + \varphi^i\right)\right] \quad (1)$$
$$i = 1,2,3,4,5$$

$I_0(x)$ is the intensity of the LASER light, $\gamma(x)$ describe the fringe contrast and $\phi(x)$ the optical phase of the wave front to be determined. φ^i is a value associated with each pixel coming from the complex interaction of the laser light with the rough surface. It can be considered as random and it is assumed that it does not vary during the experiment.

The optical phase is calculated with:

$$\tan\phi(x,y) = \frac{-2(I^4(x,y) - I^2(x,y))}{2I^3(x,y) - I^1(x,y) - I^5(x,y)} \quad (2)$$

This phase is calculated for each pixel of the image to obtain a phase map of the area of interest of the structure. This phase map is calculated for a given state of deformation. The perturbation of the structure generates a new state of deformation. A second phase map has thus to be calculated after the perturbation. The difference (pixel to pixel) of the two phase maps generates a fringe pattern containing the displacement information of the material between the two states of deformation describe by equation (3).

$$U_x(x,y) = \frac{\Delta\phi(x,y)\lambda}{4\pi\sin\theta} \quad (3)$$

$\Delta\phi(x,y)$ is the optical phase difference due to the object deformation, λ=632.8 nm the wavelength of the laser light and θ=45° is the illumination angle (Fig. 3).

Phase Shifting and Groove Machining: Application on Ultrasonic Shot-Peened Band

The specimen is an aluminum plate (AU4G) that has been ultrasonically shot-peened on a 4 mm width band, only on one side. This test specimen is then mounted on a thick T-shape notched plate (Fig. 4). It can be presumed without loss of generality that, in these conditions, the maximal residual

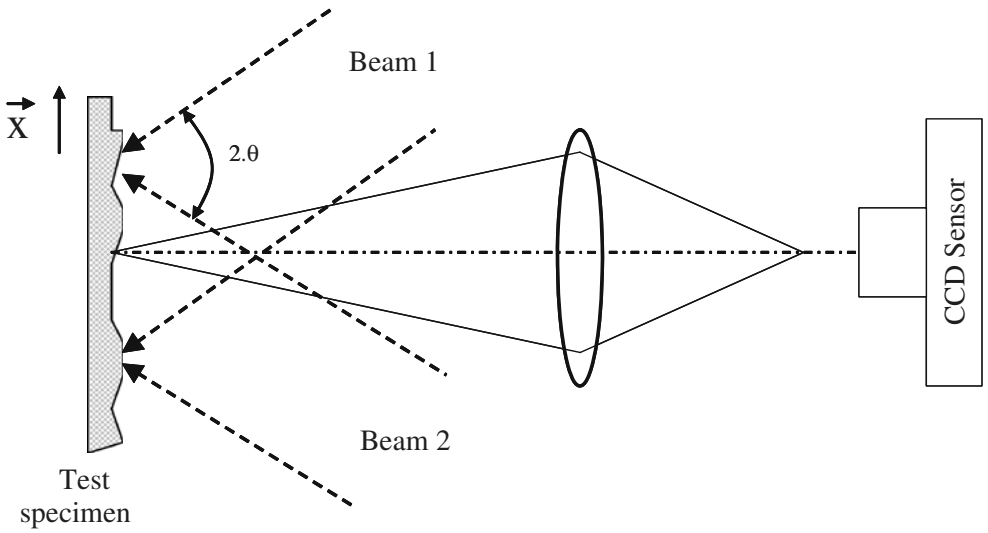

Fig. 3 Speckle interferometer for in-plane displacement measurements along direction $\vec{x}$

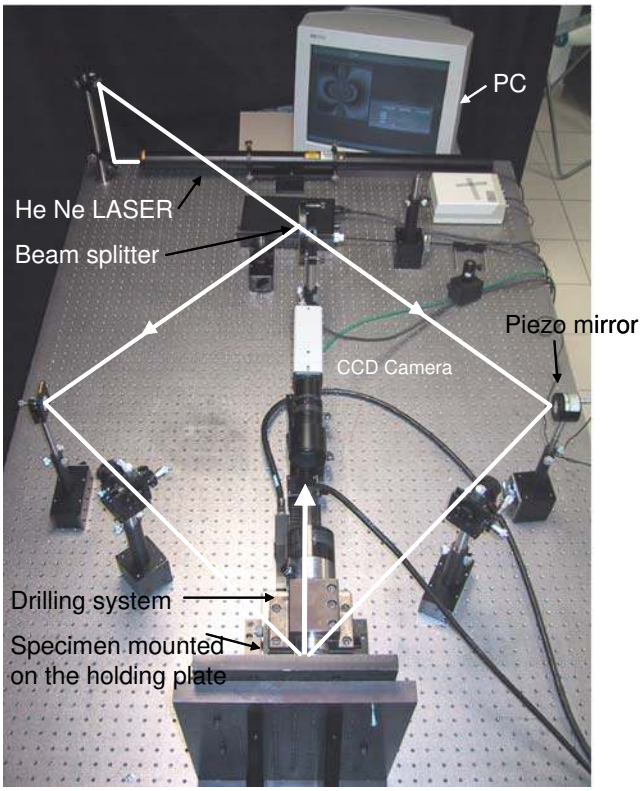

Fig. 4 Experimental set up

stress is at the centre of the band and decreases to zero while moving away from the shot peened area. Two residual stresses gradients, along y and z, are present in the structure.

The groove is machined with a milling machine mounted on a YZ translation table and locked when the position of the drill is adequate. The diameter of the tool is 2 mm and the rotation velocity is 5,000 rpm. The Y displacement of the drill is operated manually. The drilling system is then removed and the $U_x(x,y)$ displacement field is recorded by speckle interferometry. This procedure is repeated for subsequent depths increments.

The piezo mirror (a piezoelectric transducer PZT) is used to introduce phase shift. In this study, the reference image is captured in an undeformed configuration before the groove is machined. The deformed configuration is captured after each machining operation.

Figure 5 represents the phase fringes for each increment. The groove is the vertical band. The length of the groove is always the same and is considered semi-infinite with respect to the width of the prestressed area.

The size of each image is 768×576 pixels and 1 mm corresponds to 20 pixels. The width of the groove is 2 mm while the width of the shot peened band is 4 mm. On these images, the groove is vertical and the prestressed area is

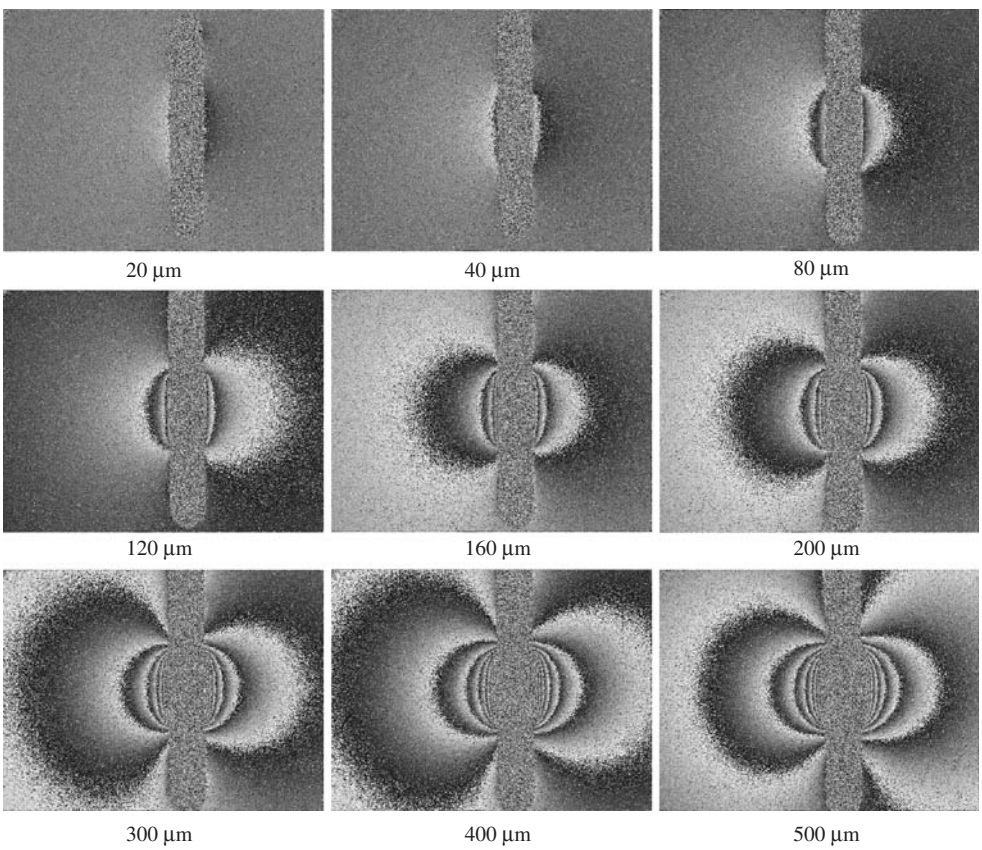

Fig. 5 Evolution of the fringe patterns as a function of the depth of the groove. The prestressed area (axis x) is horizontal

horizontal. The fringes represent the displacement $U_x(x,y)$. The sensitivity of the optical set up is 0.447 μm for a fringe order. The number of fringes increases as the depth of the groove increases. So the surface displacement increases as the depth increases and as the residual stress relaxation occurs. The problem now is to link these displacements maps to the residual stresses that were present in the structure before the machining of the groove.

It is possible to use directly the measured displacements to determine the residual stress field or the strains computed from the displacements; the latter choice has been made in the present study.

Stress Strain Relationship

A number of hypotheses have been assumed. It is considered that:

- The material behaviour is isotropic and linear elastic
- All measured displacements are continuous
- The evaluated stress is homogeneous over each cell considered.
- The residual stress determined is smaller than the elastic limit of the material
- The length of the groove is infinite compared with the dimensions of the prestressed area (Fig. 1) to neglect boundary conditions effects.
- The machining of the groove itself generates negligible displacements, this is a classical assumption for hole drilling techniques and has been verified for the present method with a stress free sample.
- The general form of the stress tensor in the shot peened band can be written as

$$\sigma = \begin{pmatrix} \sigma_x(y,z) & 0 & 0 \\ 0 & \sigma_y(y,z) & 0 \\ 0 & 0 & 0 \end{pmatrix}_{x,y,z} \quad (4)$$

This corresponds to a classical plate assumption for the stress state: the stresses on the surface of the plate and on surfaces parallel to this surface are negligible ($\sigma_{zz}=\sigma_{zy}=\sigma_{zx}=0$). Because the prestressed treatment is homogeneous and uniform on the surface, it is further considered that the shear stress is small compared to the values of σ_x and σ_y in the majority of the shot peened band.

When the groove is machined, it generates a free surface of normal x. The force $\overrightarrow{F}$ that was applied locally by the removed material on the surface element ΔS (or loaded cell presented on Fig. 6) is:

$$\overrightarrow{F} = \sigma.\overrightarrow{x}.dS = \begin{pmatrix} \sigma_x.\Delta S \\ 0 \\ 0 \end{pmatrix} \quad (5)$$

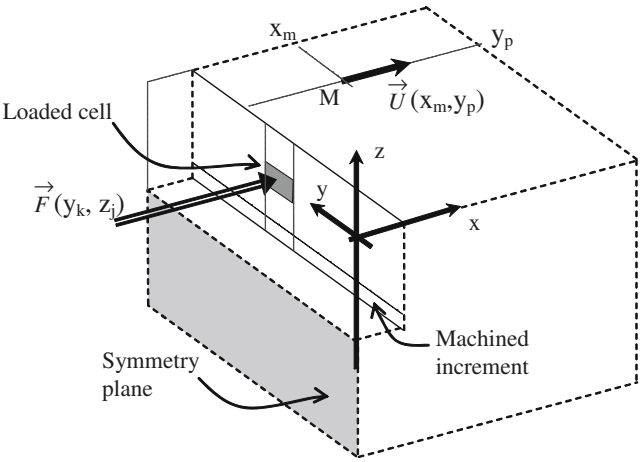

Fig. 6 Scheme of the machined groove in the component to specify the coordinates and indices

Note that the force applied on the surface of the groove is solely function of σ_x (and not σ_y) once it is admitted that the stress tensor takes the form presented in equation (4). To simplify the equations, σ_x is now written σ. Consider further the configuration presented on Fig. 6. The displacement $\overrightarrow{U}$ measured at a point $M(x_m,y_p)$ on the surface of the plate, is due to the application of the force $\overrightarrow{F}$ on the surface element centered on (y_k,z_j). Then, there is a linear relationship between $\overrightarrow{U}$ and $\overrightarrow{F}$:

$$\overrightarrow{U}(x_m,y_p) = A'(x_m,y_p,y_k,z_j).\overrightarrow{F}(y_k,z_j)$$

or

$$\begin{pmatrix} U_x(x_m,y_p) \\ U_y(x_m,y_p) \\ U_z(x_m,y_p) \end{pmatrix} = A'(x_m,y_p,y_k,z_j).\begin{pmatrix} \sigma(y_k,z_j).\Delta S \\ 0 \\ 0 \end{pmatrix} \quad (6)$$

where A' is a matrix of coefficients depending on the material properties (Young modulus and Poisson ratio), the geometry of the structure and on the respective position of M and $\overrightarrow{F}$. For the shot peened band, $\overrightarrow{F}$ corresponds to the force applied on a loaded cell and is associated to the residual stress $\sigma(y_k,z_j)$ that has been relaxed at one point of the surface of the groove (see Fig. 6). Noting

$$\varepsilon(x_m,y_p) = \frac{\partial U_x(x_m,y_p)}{\partial x} \quad (7)$$

Equation (6) is equivalent to a linear relationship between the strain $\varepsilon(x_m,y_p)$ evaluated on the surface from the displacements measured with the ESPI and the stress $\sigma(y_k,z_j)$ such that:

$$\varepsilon(x_m,y_p) = A(x_m,y_p,y_k,z_j)\sigma(y_k,z_j) \quad (8)$$

where $A(x_m,y_p,y_k,z_j)$ is a scalar calibration coefficient depending on the material properties (Young modulus and Poisson ratio), the geometry of the structure and on the respective position of M and $\overrightarrow{F}$.

When the first increment of the groove is machined, the stresses are not homogeneous along y, thus a linear combination of equations similar to equation (8) can describe the problem by superposition. Further, when the groove is machined deeper for another increment, the total value of the displacement $U_x(x_m,y_p)$ is not only due to the stresses relaxed in the current machined increment but also to the stresses relaxed in previous increments. Also, the machining of the groove generates a new stress distribution in the part and changes the geometry of the system. The relation between the measured strain field and the relaxed stress field is thus a linear combination where A becomes a matrix of coefficients, to be evaluated for each increment due to the change in the geometry of the groove. Let the indices i represent the number of increments machined into the groove, the coefficients of A depends thus also on i. If the surfaces of the plate and of the groove are now discretized, it is possible to replace the coordinates by the indices already introduced in Fig. 6 and equation (8) becomes:

$$\varepsilon^{\text{imp}} = A_{jk}^{\text{imp}} \sigma_{jk} \tag{9}$$

The upper indices are associated to the strain measurement method:

- i represents the current depth increment,
- m represents the strain coordinate in the x direction,
- p represents the strain coordinate in the y direction, that is the measurement line,

while the lower indices are related to the stress position on the face of the groove:

- k represents the loaded cell number in the y direction.
- j represents the loaded cell number in the z direction

In the examples below, only one measure of the strain is made in the x direction (m=1), thus the indices m are no longer specified in the equations.

The method is first illustrated with a case study presented on Fig. 7. The problem is here discretized for the first groove increment (i=1) with a specific simplified geometry whose generalization will be discussed in subsequent parts of this work. Consider three cells of equal areas on the surface of the groove loaded with σ_{11}, σ_{12}, and σ_{13}, constant normal stresses on each respective cell. Consider further three strains ε^{11}, ε^{12} and ε^{13} measured on the surface of the plate, on three lines (defined by y equal constant) issuing from the middle of the border of each cell at a given m=1 position as specified on Fig. 7. Then, by

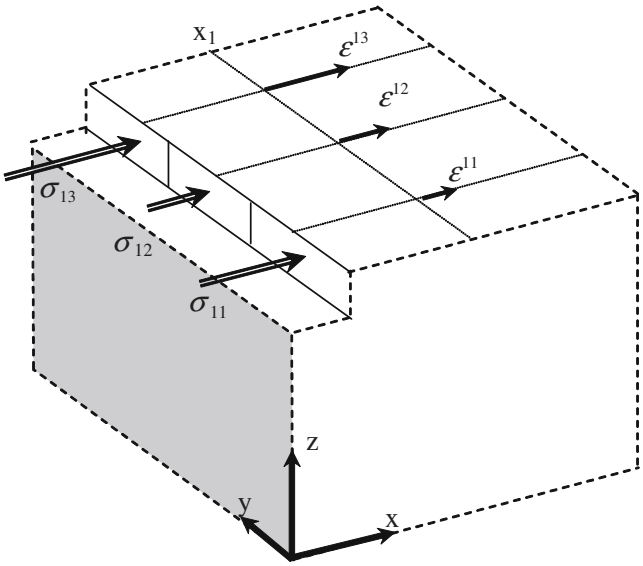

Fig. 7 Simple discretization for the first groove increment (i=1)

superposition, it is possible to construct an equation whose solution is σ_{11}, σ_{12}, σ_{13}:

$$\begin{pmatrix} A_{11}^{11} & A_{12}^{11} & A_{13}^{11} \\ A_{11}^{12} & A_{12}^{12} & A_{13}^{12} \\ A_{11}^{13} & A_{12}^{13} & A_{13}^{13} \end{pmatrix} . \begin{pmatrix} \sigma_{11} \\ \sigma_{12} \\ \sigma_{13} \end{pmatrix} = \begin{pmatrix} \varepsilon^{11} \\ \varepsilon^{12} \\ \varepsilon^{13} \end{pmatrix} \text{ or } \sum_{k=1}^{3} A_{1k}^{1p} . \sigma_{1k} = \varepsilon^{1p} \tag{10}$$

The indices have the same signification as for equation (9). Considering that the length of the groove is infinite, there is no effect of the groove edges on the coefficients. Consider further that each cell is charged alternatively with a unit stress, it can be deduced from the geometrical regularity of the system:

$$\begin{aligned} A_{11}^{11} &= A_{12}^{12} = A_{13}^{13} \\ A_{11}^{12} &= A_{12}^{11} = A_{12}^{13} = A_{13}^{12} \\ A_{11}^{13} &= A_{13}^{11} \end{aligned} \tag{11}$$

This could be repeated for any number of loaded cells as long as the area of the cells are equal to the reference cell and the strain is evaluated at the same relative position. Under such conditions, only one finite element simulation is necessary corresponding to a unit load on a unique cell and the matrix A is symmetric, which simplifies the inversion of equation (10).

Note that it is not necessary that the cells be of equal area and that the strains be measured at any specific positions. For these cases, equation (10) remains valid, but each of the coefficients of A are to be determined individually and the matrix is no longer symmetric.

Computation of the Calibration Coefficients

When the matrix A is symmetric, the calibration coefficients are obtained through a single finite element analysis by

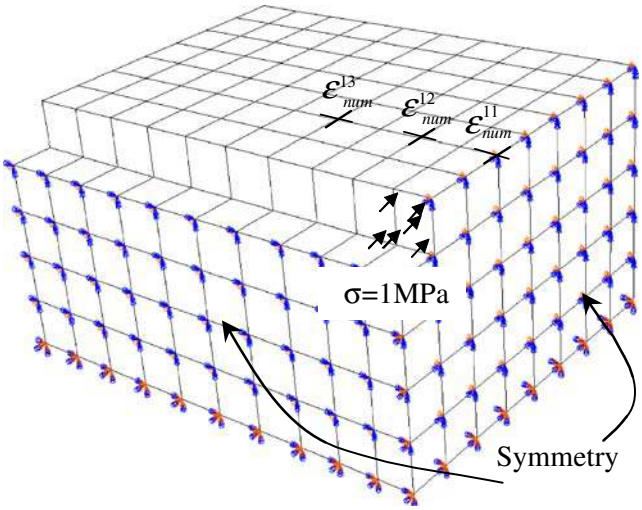

Fig. 8 Load and boundary conditions applied in the finite elements model

loading a cell with a unique unit stress σ=1 MP and calculating the corresponding strains. Figure 8 represents a scheme of the load applied in the finite element model. The model for the part is sufficiently large to warranty that the groove can be considered infinite. Only one quarter of the structure is modeled due to the symmetry of the structure and the symmetry of the load. The finite element mesh is composed with 390 C3D8 elements, the bottom nodes of the solid are fixed, the load and symmetric conditions are imposed as presented on Fig. 8. Figure 9 presents the results obtained for the x component of the displacement field computed with the finite element simulation. It can be seen that the displacements tend to zero away from the loaded cell, which confirms that the model is equivalent to an infinite groove. The coefficients are then given with

$$A_{11}^{11} = \frac{\varepsilon_{\text{num}}^{11}}{\sigma}, A_{11}^{12} = \frac{\varepsilon_{\text{num}}^{12}}{\sigma}, A_{11}^{13} = \frac{\varepsilon_{\text{num}}^{13}}{\sigma} \tag{12}$$

where $\varepsilon_{\text{num}}^{11}$, $\varepsilon_{\text{num}}^{12}$ and $\varepsilon_{\text{num}}^{13}$ are the numerical strains determined at the predefined positions (mp), and num indicates a numerical value computed with the finite element method; σ is the stress value of the stress applied in the finite element computation (1 MPa). Once the coefficients are defined, equation (10) can be inversed to find the stress field:

$$\cdot \begin{pmatrix} \sigma_{11} \\ \sigma_{12} \\ \sigma_{13} \end{pmatrix} = \begin{pmatrix} A_{11}^{11} & A_{12}^{11} & A_{13}^{11} \\ A_{11}^{12} & A_{12}^{12} & A_{13}^{12} \\ A_{11}^{13} & A_{12}^{13} & A_{13}^{13} \end{pmatrix}^{-1} \begin{pmatrix} \varepsilon_{\text{exp}}^{11} \\ \varepsilon_{\text{exp}}^{12} \\ \varepsilon_{\text{exp}}^{13} \end{pmatrix} \tag{13}$$

where $\varepsilon_{\text{exp}}^{11}$, $\varepsilon_{\text{exp}}^{12}$ and $\varepsilon_{\text{exp}}^{13}$ are now the strains evaluated from the experimental displacements (indicated by exp) and evaluated at the same predefined positions than their numerical counterparts.

Stress Strain Relationship for the Second Groove Increment

For the second increment machined, the new residual stress distribution due to the first increment must be taken into account (see Fig. 10). Indeed, the fact that the stresses relax during the previous machining, generates a new stress distribution in the solid when it is the initial one that is sought for. Further, there is a new set of coefficients for each geometry of the groove. For the simple geometry of the example chosen (see Fig. 10), the measured strains are

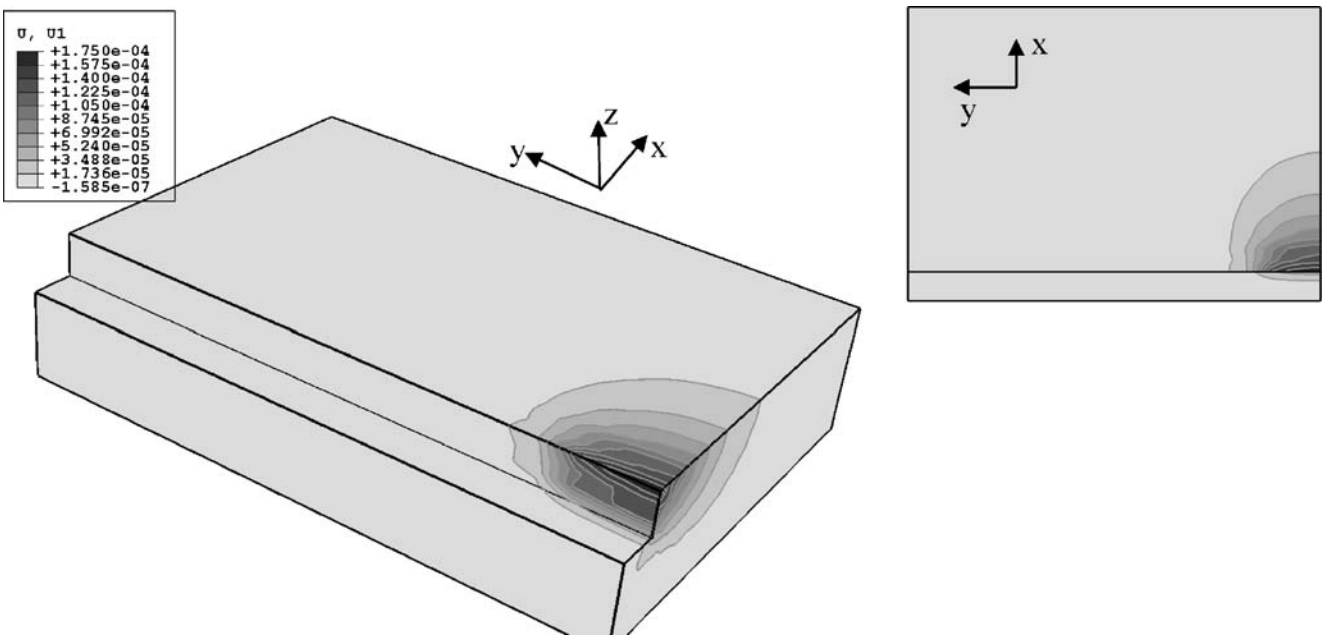

Fig. 9 Numerical displacement $U_x(x,y)$ for the first step drilled

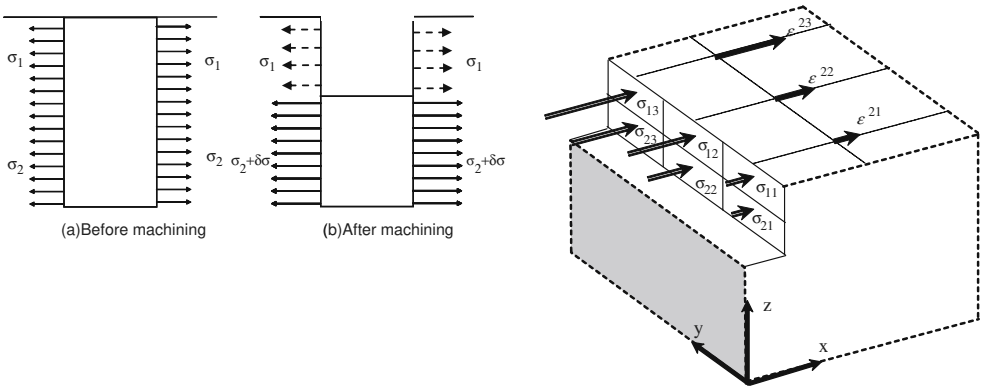

Fig. 10 Scheme of the new in depth stress distribution in depth for the second groove increment (i=2)

now the consequences of the relaxation of the two rows of cells. The residual stress σ_2 is affected by the new distribution of stress and by the new geometry of the structure it can be seen that equation (16) take in account this contribution $\delta\sigma$. This means that they are a function of the six stress values through coefficients that are different from the one computed for the first increment. For the second increment machined, as presented on Fig. 10, the strains ε^{21}, ε^{22} and ε^{23} on the surface are by superposition:

$$\begin{pmatrix}\varepsilon^{21}\\ \varepsilon^{22}\\ \varepsilon^{23}\end{pmatrix} = \begin{pmatrix}A_{11}^{21} & A_{12}^{21} & A_{13}^{21}\\ A_{11}^{22} & A_{12}^{22} & A_{13}^{22}\\ A_{11}^{23} & A_{12}^{23} & A_{13}^{23}\end{pmatrix}.\begin{pmatrix}\sigma_{11}\\ \sigma_{12}\\ \sigma_{13}\end{pmatrix} + \begin{pmatrix}A_{21}^{21} & A_{22}^{21} & A_{23}^{21}\\ A_{21}^{22} & A_{22}^{22} & A_{23}^{22}\\ A_{21}^{23} & A_{22}^{23} & A_{23}^{23}\end{pmatrix}.\begin{pmatrix}\sigma_{21}\\ \sigma_{22}\\ \sigma_{23}\end{pmatrix} \quad (14)$$

or

$$\sum_{j=1}^{2}\left(\sum_{k=1}^{3} A_{jk}^{ip}.\sigma_{jk}\right) = \varepsilon^{ip} \quad (15)$$

The stresses σ_{11}, σ_{12}, σ_{13} are known from the first increment. The residual stresses that where present in the structure before the machining can be obtained with:

$$\begin{pmatrix}\sigma_{21}\\ \sigma_{22}\\ \sigma_{23}\end{pmatrix} = \begin{pmatrix}A_{21}^{21} & A_{22}^{21} & A_{23}^{21}\\ A_{21}^{22} & A_{22}^{22} & A_{23}^{22}\\ A_{21}^{23} & A_{22}^{23} & A_{23}^{23}\end{pmatrix}^{-1} .\left(\begin{pmatrix}\varepsilon^{21}\\ \varepsilon^{22}\\ \varepsilon^{23}\end{pmatrix} - \begin{pmatrix}A_{11}^{21} & A_{12}^{21} & A_{13}^{21}\\ A_{11}^{22} & A_{12}^{22} & A_{13}^{22}\\ A_{11}^{23} & A_{12}^{23} & A_{13}^{23}\end{pmatrix}.\begin{pmatrix}\sigma_{11}\\ \sigma_{12}\\ \sigma_{13}\end{pmatrix}\right) \quad (16)$$

The same type of finite element analysis as for the first increment can be performed to find the new set of coefficients. The matrices will conserve their symmetry as long as the areas of the cells are equal and the strains are measured at predefined positions. It can be further noted that equation (16) is general: the size of the cells for the second increment can be arbitrary and not necessarily connected to the size of the cells of the first row if the coefficients are to be computed individually.

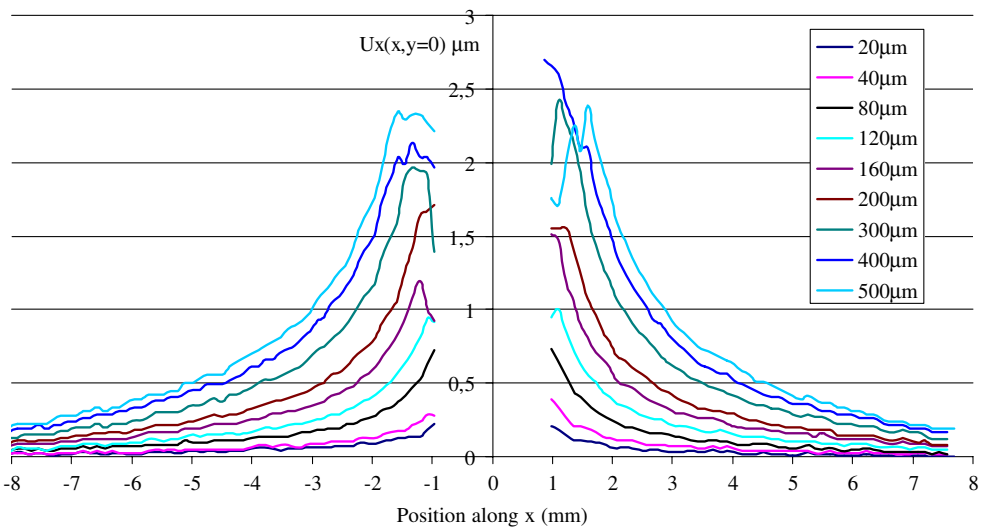

Fig. 11 Measured displacement along the centre line (y=0) of the prestressed area for various machining increments from 20 to 500 µm

Stress Strain Relationship in the General Case

In the general case and for subsequent groove increments, a number K of cells is considered for a total of I increments machined. The number of lines on which the strains are measured is P. This gives a number $I \times K$ unknown stress values to be obtained from a number $I \times P$ strain measurements. When the first increment is machined, it comes

$$\varepsilon^{1p} = \sum_{k=1}^{K} A_{1k}^{1p} . \sigma_{1k} \tag{17}$$

When increment i is machined:

$$\varepsilon^{ip} = \sum_{k=1}^{K} A_{ik}^{ip} . \sigma_{ik} + \sum_{j=1}^{i-1} \sum_{k=1}^{K} A_{jk}^{ip} . \sigma_{jk} \tag{18}$$

The term $\sum_{k=1}^{K} A_{ik}^{ip} . \sigma_{ik}$ of this last equation contains the K unknown stresses σ_{ik} of the current increment (number i) as a function of the measured strains ε^{ip} and of the stresses calculated for the previous increments $\sum_{j=1}^{i-1} \sum_{k=1}^{K} A_{jk}^{ip} . \sigma_{jk}$. This term describes the stress redistribution in layer i due to previous machining increments.

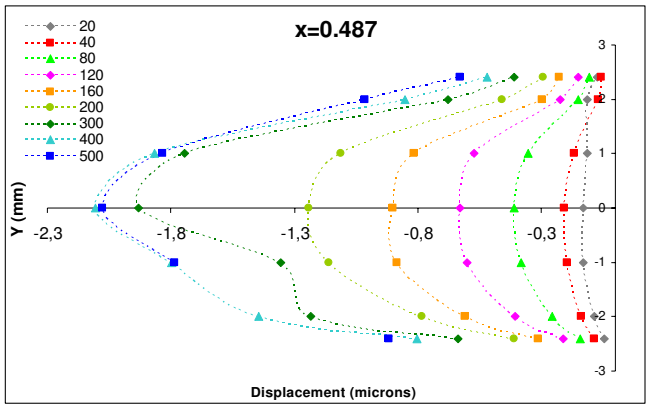

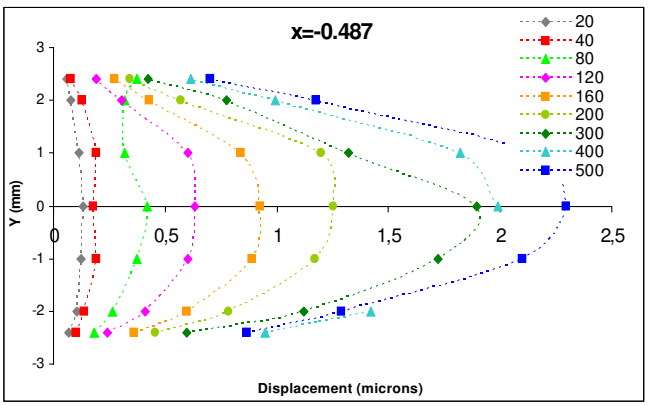

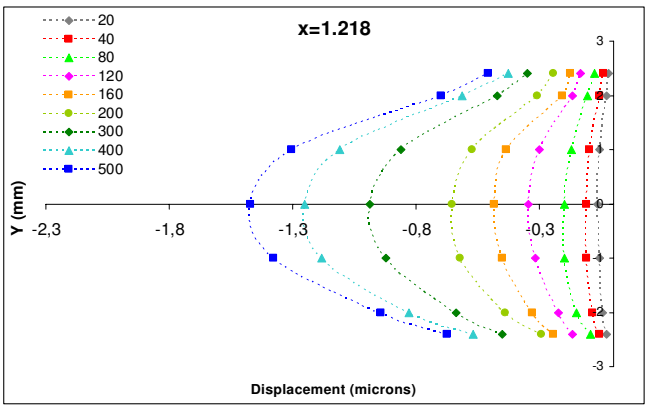

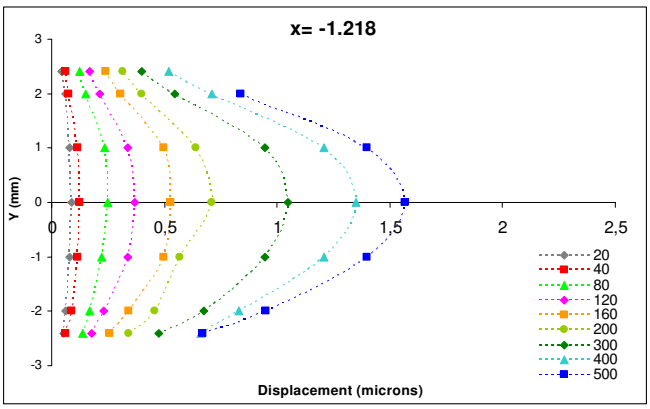

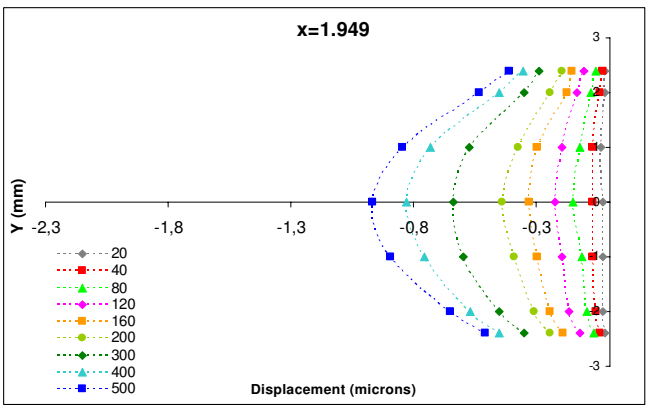

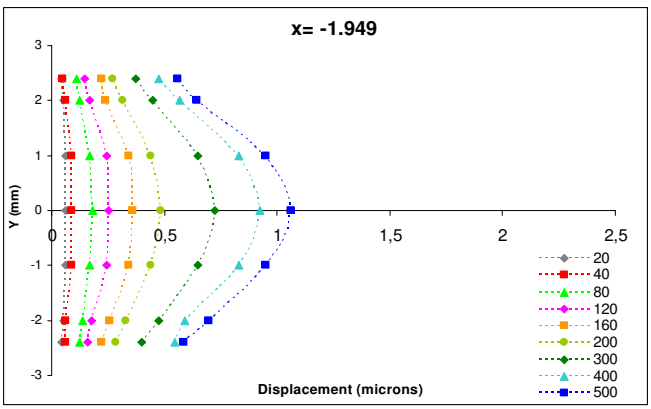

Surface displacement on the left part of the groove

Surface displacement on the right part of the groove

Fig. 12 Surface displacement on the two parts (*left and right*) of the groove as a function of the position x and as a function of the depth

If the number P of measurement lines is equal to the number K of cells, the system of equation (18) can in general be inverted directly. It can be noted that the number of lines P where the strains are evaluated does not have to be equal to the number of cells K. Ideally P should be higher than J: this would mean that there are several measured strains at a given x for each stress cell, increasing the number of experimental data to determine the stress and thus minimizing uncertainties on the results. The method presented above can be generalized for this situation but looses its geometrical convenience. If the number P of measurement lines is larger than K, then, the system [equation (18)] can be solved with the help of a least square procedure.

All the above discussion was done for strain measurements at a given single distance x_m from the groove centre (m=1) in equation (9) but it can be generalized to an arbitrary number of measurement points on each line as well, taking the indices m into account. Similar relations can also be obtained to relate stresses and displacements instead of strains.

Results

In this study, the indices i, j, k and p proposed by the authors are:

- $1<i<9$; $I=9$ in depth machined increments,
- $1<j<I$, $1<k<6$ ($K=6$) that is a total of $I\times K=54$ stress cells,
- $1<p<6$; $P=6$ measurement lines with $P=K$.

Figure 11 represents the displacements measured with the ESPI in the centre of the prestressed area ($y=0$). The displacements are given for the nine increments drilled and on the left and on the right of the groove. We can note a good symmetry in the displacement field, except very close to the groove for the last three increments. This symmetry in the displacement field proves that the tools axis is perpendicular to the surface. This symmetry can also be seen in the fringe patterns (see Fig. 5). Figure 12 shows an example of the displacement field $U_x(x,y)$ obtained as a function of the depth and for three positions along x.

To calculate the strain, two positions are chosen for the displacements: $x=1.8$ mm and $x=3.3$ mm. These measurement points have been chosen far enough from the groove not to be affected by the eventual plastified area due to the machining. The strain is calculate with:

$$\varepsilon = \frac{U_x(x=1.8,y) - U_x(x=3.3,y)}{L} \qquad (19)$$

L is the distance between the two points ($L=1.5$ mm). The same points are used in the finite element simulation to compute the calibration coefficients. For each increment, the displacement is extracted for the six positions in the direction y. The influence of the shot peened area (-2 mm$<y<+2$ mm) on the value of the displacement can be observed on Fig. 12. The displacement magnitude decreases while moving away from the prestressed area.

The residual stress profiles along the direction y and along the depth are presented in Fig. 13. It can be seen that the prestressed area extends beyond the treated area: out of this area the residual stress is not equal to zero but decreases while moving away from the prestressed area: for 2 mm$<y<$3 mm a residual stress gradient exists indeed in the structure.

Conclusion

A new approach in residual stress analysis based on the combination of an optical and a mechanical setup is proposed. The results presented confirm the feasibility of this approach, which has next to be compared to other stress evaluation methods. Sources of uncertainty and error and estimation of their magnitude will be presented in a future paper. The originality of the technique is the possibility to measure both the stress profile in the depth of the structure, and the stress profile along the axis of the machined groove. This can be useful to measure stress gradients in two directions, for instance in welded joints. With this technique, the influence of a prestressed area, larger than the treated area, was estimated accurately. An advantageous choice of geometry can further be performed to limit the number of finite element computations. These results have been determined with a minimum of measurements, only with a small groove in the structure, which classifies this method as semi-destructive.

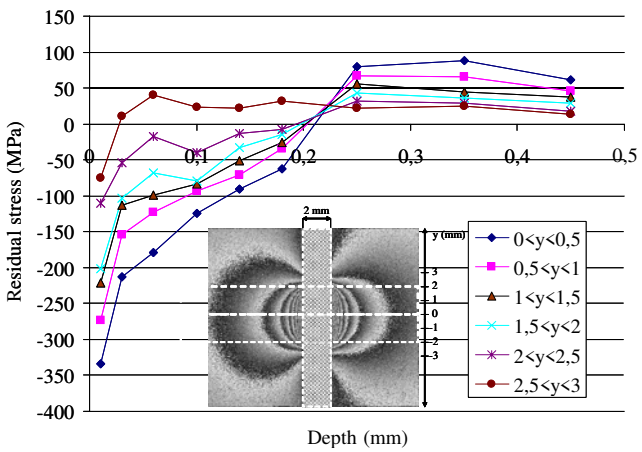

Fig. 13 Residual stress field results

References

1. Lu J (1996) Handbook of measurements of residual stress. SEM, Edited by Jian Lu
2. Lu J (2005) Handbook on residual stresses. Second edition, Volume 1 Residual stress: manufacturing and materials processing. Volume 2. Residual stress and mechanical design. SEM, edited by Jian Lu
3. Hauk V (1997) Structural and residual stress analysis by non destructive methods. Elsvier
4. Hathaway RB, Hovanesian JD, Hung MYY (1997) Residual stress evaluation using shearography with large-shear displacements. Opt Lasers Eng 271:43–60.
5. Montay G, Bulhak J, Surrel Y, Vautrin A, Lu J (2005) Use of full field of strains found by grating shearography to determine residual stress. J Strain Anal Eng Des 407:621–630.
6. Schajer GS, Steinzig M (2005) Full-field calculation of hole drilling residual stresses from electronic speckle pattern interferometry data. Exp Mech 456:526–532.
7. Wu Z, Lu J, Han B (1998) Study of residual stress distribution by a combined method of Moire interferometry and incremental hole drilling, Part I: Theory. J Appl Mech-Trans ASME 654:837–843.
8. Wu Z, Lu J, Han B (1998) Study of residual stress distribution by a combined method of Moire interferometry and incremental hole drilling, part II: implementation. J Appl Mech-Trans ASME 654:844–850.
9. Ya M, Marquette P, Belahcene F, Lu J (2004) Residual stresses in laser welded aluminium plate by use of ultrasonic and optical methods. Mater Sci Eng, A Struct Mater Prop Microstruct Process 3821–2:257–264.
10. Duquennoy M, Ouaftouh M, Qian ML, Jenot F, Ourak M (2001) Ultrasonic characterization of residual stresses in steel rods using a laser line source and piezoelectric transducers. NDT E Int 345:355–362.
11. Montay G, Cherouat A, Lu J, Baradel N, Bianchi L (2002) Development of high precision incremental step hole drilling method for the study of residual stress in multi-layer materials: influence of temperature and substrate on ZrO_2–Y_2O_3 8 wt.% coating. Surf Coat Technol 155155/2–3:152–160.
12. Makino A, Nelson DV (1994) Residual stress determination by single-axis holographic interferometry and hole drilling method. Exp Mech 341:66–78.
13. Prime MB, Sebring RJ, Edwards JM, Hughes DJ, Webster PJ (2004) Laser surface-contouring and spline data-smoothing for residual stress measurement. Exp Mech 442:176–184.
14. Prime MB (2006) Erratum to “laser surface-contouring and spline data-smoothing for residual stress measurement. Exp Mech 445:541.
15. Prime MB (2001) Cross-sectional mapping of residual stresses by measuring the surface contour after a cut. J Eng Mater Technol 1232:162–168.
16. Hill MR, Lin WY (2002) Residual stress measurement in a ceramic-metallic graded material. J Eng Mater Technol-Trans ASME 1242:185–191.
17. Schajer GS, Prime MB (2007) Residual stress solution extrapolation for the slitting method using equilibrium constraints. J Eng Mater Technol-Trans ASME 1292:227–232.
18. Cloud G (1995) Optical methods of engineering analysis. Cambridge University Press, New York.
19. Jones R, Wykes C (1989) Holographic and speckle interferometry. 2nd edn. Cambridge University Press
20. Nicoletto G (1991) Moire interferometry determination of residual stresses in the presence of gradients. Exp Mech 313:252–256.
21. Kaufmann GH, Galizzi GE (2002) Phase measurement in temporal speckle pattern interferometry: comparison between the phase-shifting and the Fourier transform methods. Appl Opt 4134:7254–7263.